Biomaterials 31 (2010) 9031–9039

Contents lists available at ScienceDirect

Biomaterials

journal homepage: www.elsevier.com/locate/biomaterials

# The effect of nanofiber-guided cell alignment on the preferential differentiation of neural stem cells

Shawn H. Lim [a], Xingyu Y. Liu [b,c], Hongjun Song [c], Kevin J. Yarema [a], Hai-Quan Mao [b,*]

[a] Department of Biomedical Engineering, Johns Hopkins University School of Medicine, 3400 N. Charles St., Baltimore, MD 21218, USA
[b] Department of Materials Science and Engineering and Whitaker Biomedical Engineering Institute, Johns Hopkins University, 3400 N. Charles St., Baltimore, MD 21218, USA
[c] Institute of Cell Engineering and Departments of Neurology and Neuroscience, Johns Hopkins University School of Medicine, 720 Rutland Avenue, Baltimore, MD 21205, USA

ARTICLE INFO

*Article history:*
Received 21 July 2010
Accepted 7 August 2010
Available online 24 August 2010

*Keywords:*
Neural stem cell
Differentiation
Aligned nanofiber
Electrospun fiber

ABSTRACT

Stem cells display sensitivity to substrate presentation of topographical cues via changes in cell morphology. These biomechanical responses may be transmitted to the nucleus through cytoskeletal-linked signaling pathways. Here we investigate the influence of aligned substratum topography on the cell morphology and subsequently, the neuronal differentiation capabilities of adult neural stem cells (ANSCs). ANSCs that were cultured on aligned fibers elongated along the major fiber axis. Upon induction of differentiation with retinoic acid, a higher fraction of cells on aligned fibers exhibited markers of neuronal differentiation as compared with cells on random fiber or unpatterned surfaces. This effect was in part due to substrate selectivity, whereby aligned fiber substrates were less receptive to the attachment and continued survival of oligodendrocytes than random fiber or unpatterned substrates. Substrate-induced elongation alone was also effective in upregulating canonical Wnt signaling in ANSCs, which was further potentiated by retinoic acid treatment. These findings suggest a mechanism by which morphological control of stem cells operates in concert with biochemical cues for cell fate determination.

© 2010 Elsevier Ltd. All rights reserved.

## 1. Introduction

Stem cell therapies in regenerative medicine can often be complemented by a supportive scaffold that fills the injury site and assists in tissue repair [1–4]. Knowledge of how cell fate can be mediated by substrate properties paves way for the rational design of synthetic scaffolds for *de novo* tissue regeneration. Regulatory cues within the stem cell niche include growth factors, cell–cell interactions, or cell–matrix adhesions, which have traditionally been characterized as biochemical in nature. On the other hand, there has been increasing attention devoted to how the physical properties of the stem cell microenvironment influence cell fate. Preferential differentiation and cell maturation towards a specific lineage can be enhanced by various physical stimuli. Recent exciting work has demonstrated that fate choice of mesenchymal stem cells (MSCs) can be specified by altering parameters such as substrate stiffness or cell shape [5–7]. These results clearly indicate that cells are capable of detecting biomechanical properties of the underlying substrate, and alter their morphology accordingly via rearrangement of cytoskeletal components such as actin structures and focal adhesion complexes, thus facilitating a conversion of the extrinsic mechanical signal into initiation of intracellular signaling. Groups of cytoskeletal-associated molecules have been identified as potential upstream effectors of such substrate-induced signaling [8–10]. However, the majority of the intermediary steps connecting cytoskeletal remodeling to specific transcription pathways at the nuclear level remain to be elucidated.

Biomechanical cues can also be transmitted to cells via micro or nanoscale substrate topography. Morphological and functional changes have been observed for various types of cells, including MSCs, when cultured on substrates presenting topographical features such as pillars, grooves, or pits [11–13]. Furthermore, these changes were regulated in a feature size-dependent manner. Since distinct morphological characteristics often accompany stem cell differentiation, the question of whether one can conversely utilize topography-induced alterations in cell morphology to impact stem cell fate choices becomes scientifically interesting and relevant.

In this study, we assessed the potential of these substrate-presented topographical features to influence differentiation fate specification using multipotent adult neural stem cells (ANSCs) as a model cell line. We investigated whether cell morphology changes (e.g. elongation along a single axis) induced by a submicron-sized,

* Corresponding author. Tel.: +1 (410) 516 8792; fax: +1 (410) 516 5293.
*E-mail address:* hmao@jhu.edu (H.-Q. Mao).

0142-9612/$ – see front matter © 2010 Elsevier Ltd. All rights reserved.
doi:10.1016/j.biomaterials.2010.08.021

aligned substrate would result in a differential response to exogenously applied chemical cues as compared with randomly patterned or planar unpatterned substrates. Fibers with a range of diameters were produced so as to be able to investigate the impact of different feature sizes on cellular cell adhesion, survival and differentiation. We also examined differential signaling activation of the Wnt/β-catenin pathway in cells on fiber substrates, as it has been shown to correlate with increased neurogenesis in ANSCs [14].

## 2. Materials and methods

### 2.1. Electrospinning of fiber meshes

Polycaprolactone (PCL, Mw 70 kDa, Sigma–Aldrich, St. Louis, MO) was used to fabricate the electrospun fibrous scaffolds. Solutions of 12–15 wt% PCL were prepared by dissolving the pellets in a mixture of 4:1 dichloromethane/methanol. Nanofibrous scaffolds were formed by doping 1% wt/(wt polymer) octadecyl rhodamine B chloride (R18, Invitrogen, Carlsbad, CA) into 12 wt% PCL solution prior to electrospinning [15]. The polymer solution was dispensed from a syringe pump at a flow rate of 2.5 ml/h through a blunted 27G syringe needle; at the same time, a 12 kV electric potential was applied to the needle from a high voltage power supply. Fiber deposition onto a stationary grounded collector results in random fiber meshes, while a rotating disc collector yielded aligned fiber meshes [16]. For cell culture studies, ~20 μm-thick fiber layers were deposited onto 15 mm glass coverslips and affixed with a small amount of biocompatible silicone adhesive (Factor II, Lakeside, AZ). PCL films were also fabricated as a flat, two-dimensional substrate by spin coating coverslips with 1% PCL dissolved in dichloromethane.

### 2.2. Fiber diameter analysis

Electrospun fibers with different average fiber diameters were achieved through variation of the concentration of polymer solution or via doping with R18 as described above. Fiber meshes were sputter-coated with 4 nm of platinum prior to being imaged at high magnification using scanning electron microscopy (SEM; JEOL 6700F, Tokyo, Japan). Fiber diameters were measured from SEM micrographs using NIH ImageJ software. A minimum of 100 fibers were measured to obtain the average fiber diameter for the sample.

### 2.3. Cell culture and ANSC differentiation

ANSCs were derived from the hippocampus of adult Fischer 344 rats and infected with retroviruses to express GFP as described previously [17]. Cells were propagated on polyornithine (PLO)/laminin (Sigma–Aldrich) coated tissue culture flasks in DMEM/F12 media containing N2 supplement (Invitrogen) and 20 ng/ml FGF-2 (Peprotech, Rocky Hill, NJ). Under these conditions, over 90% of ANSCs stain positively for the neural progenitor marker nestin. These ANSCs have been shown to give rise to electrically active and functional neurons *in vitro* [18] and give rise to neurons and glia after transplantation *in vivo* [19].

Prior to seeding with cells, fiber meshes on coverslips were sterilized by a series of washing steps in 70% ethanol followed by sterile Milli-Q water, and then sequentially coated with PLO (10 μg/ml, 37 °C for 2 h) and laminin (20 μg/ml, 37 °C overnight). For neuronal differentiation studies, ANSCs were first seeded at a concentration of 12,500 cells/cm$^2$ (25,000 cells/coverslip) in DMEM/F12/N2 media containing 1 ng/ml FGF-2 and allowed to attach for 24 h. Differentiation was initiated via treatment with 0.5 μM retinoic acid (RA) and 0.5% fetal bovine serum (FBS) [20]. After further five days in culture, the cells were fixed for immunostaining and further analysis. To evaluate the impact of higher density culture on neuronal differentiation from ANSCs, the same procedure was repeated, except that the initial seeding density used was 30,000 cells/cm$^2$. For oligodendrocyte attachment and survival studies, ANSCs in tissue culture flasks were treated with 100 ng/ml noggin (Peprotech) and 100 ng/ml IGF-1 (Peprotech) and allowed to differentiate for five days [21]. Cells were then trypsinized and re-plated onto fiber substrates or PLO/LN-coated 24-well tissue culture plates at a density of 25,000 cells/cm$^2$, and cultured for an additional 48 h before fixation and immunostaining.

### 2.4. Immunofluorescence staining and imaging

Cells were fixed with 4% paraformaldehyde at 4 °C for 30 min and then permeabilized and blocked with 1× Tris-buffered saline (TBS) containing 5% goat serum and 0.05% Triton X-100 for 90 min. Samples were incubated with the relevant primary antibodies overnight at 4 °C, washed with TBS, and then incubated with fluorophore-tagged secondary antibodies for 90 min at room temperature. DAPI or SYTOX Green (Invitrogen) staining was used for visualization of cell nuclei. The primary antibodies used were specific against nestin (undifferentiated ANSCs, Millipore, Billerica, MA), Tuj1 (immature neurons, Covance, Princeton, NJ), RIP (oligodendrocytes, Iowa Developmental Studies Hybridoma Bank), GFAP (astrocytes, Dako, Denmark), Ki-67 (proliferating cells, Novocastra, Newcastle, UK). The secondary antibodies used were anti-rabbit and anti-mouse Alexa Fluor 488 and 546 (Invitrogen). Apoptotic cell detection and staining (TUNEL assay) was performed using a fluorescein *in situ* cell death detection kit (Roche Applied Science, Indianapolis, IN) according to the manufacturer's instructions. Samples were imaged using a Nikon TE2000 epifluorescence microscope. Images were captured at 100× and 200× for manual counting of positively stained cells. A minimum of 1000 cells were counted for each sample using NIH ImageJ software with 5 replicates for each type of fiber substrate and experimental condition.

### 2.5. WST-1 cell viability assay

Cell viability after seeding onto the substrates was indirectly assessed via quantification of their metabolic activity using the WST-1 cell proliferation assay (Roche Applied Science) according to the manufacturer's instructions. Briefly, WST-1 reagent was incubated with normal cell media at 1:10 dilution for 4 h at 37 °C. Cleavage of tetrazolium salt in the reagent yields a soluble formazan dye whose rate of production correlates with mitochondrial activity, and can be quantified via measuring absorbance at 450 nm. Sample absorbance values were converted to absolute cell number by correlating with a standard curve.

### 2.6. Wnt signaling

A luciferase reporter assay was used to measure the level of activation of Wnt signaling through the canonical Wnt/β-catenin pathway [22]. Samples of pGL3-OT and pGL3-OF plasmids were a kind gift from the lab of Dr. Bert Vogelstein and Dr. Kenneth Kinzler at the Johns Hopkins University School of Medicine. Plasmids were expanded from transformed DH5α cultures and purified with a Plasmid Giga Kit (Qiagen, Valencia, CA). ANSCs were transiently transfected using Lipofectamine 2000™ (Invitrogen), then trypsinized and re-seeded onto fiber substrates at a concentration of 50,000 cells/cm$^2$. Cells were treated with RA/FBS or recombinant Wnt3a (R&D Systems, Minneapolis, MN), incubated for a further 24 h, and then lysed and assayed for luciferase activity using a luciferase assay kit (Promega, Madison, WI). Relative light unit values (RLU) from the cells in each sample were normalized to the

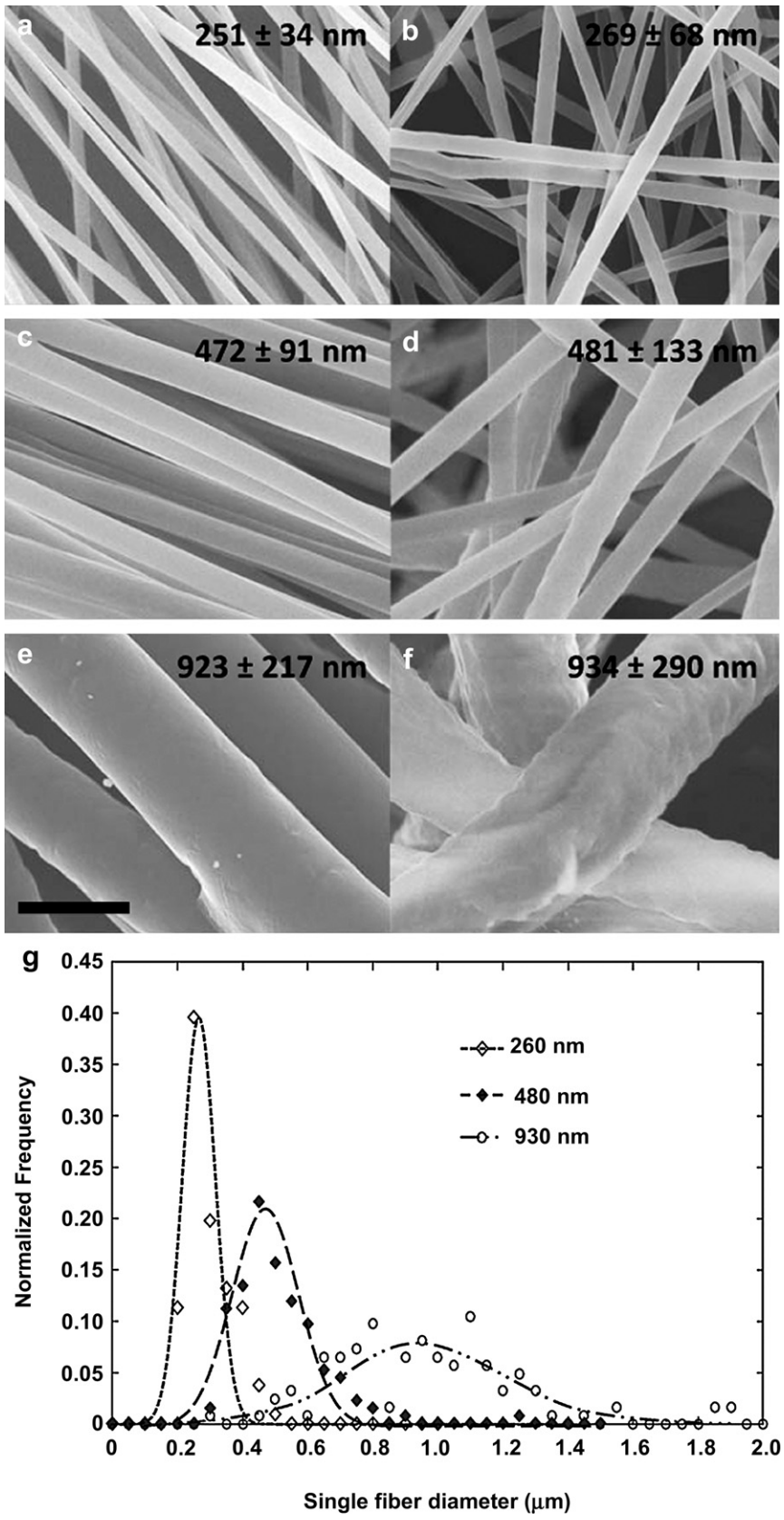


**Fig. 1.** SEM images of aligned and random electrospun PCL fiber meshes; images were acquired at 10000×, scale bar = 1 μm. Fibers were electrospun from 12 wt%/R18 solution (a, b); 12 wt% solution (c, d); 14 wt% solution (e, f). The average fiber diameter for each condition is noted on the figure. (g) Histogram of fiber diameter distribution at each solution concentration, combining the diameters of aligned and random fibers. An approximate diameter value (260 nm, 480 nm, 930 nm) was used to refer to each of the groups in the text.

total protein in the sample, and then further represented as the fold-increase over luciferase activity in cells seeded on 2D substrates without any biochemical treatment.

### 2.7. Statistical analysis

Values are represented on the bar graphs as the average ± s.e.m. Statistical significance was determined using the Student's t-test for pairwise analysis, where values of $p < 0.05$ were considered statistically significant.

## 3. Results

### 3.1. Characterization of electrospun fibers

Electrospinning was employed to fabricate both aligned and random fiber meshes with different average fiber diameters. Aligned fibers were achieved by directing the charged polymer jet towards the edge of a rapidly rotating metal disc collector (Fig. 1a, c, e). Conversely, deposition onto a stationary collector yielded random fiber meshes due to the whipping instability of the jet caused by electrostatic repulsion on its surface (Fig. 1b, d, f). As shown in Fig. 1, decreasing the polymer solution concentration from 14 wt% to 12 wt% was sufficient to reduce the average fiber diameter by half, and addition of the cationic amphiphile R18 successfully decreased the average diameter and narrowed the diameter distribution profile, as previously reported [15], likely due to the reduction in surface tension of the polymer jet with decreasing polymer concentration. Although the addition of the fluorescent R18 resulted in pink-dyed fibers, the molecule was easily leached out by washing with ethanol prior to cell culture, without negative impact on the individual fiber stability and morphology (data not shown). Furthermore, any residual amount of R18 was sufficiently negligible so as not to interfere with later immunostaining experiments. Electrospinning of 12 wt%/R18, 12 wt %, and 14 wt% PCL solutions yielded fibers with average diameters of approximately 260 nm, 480 nm and 930 nm, respectively (and are referred to as thus for the remainder of the text). The specific average diameters for aligned and random fibers at each concentration were virtually the same and are listed in Fig. 1.

### 3.2. Neuronal differentiation of ANSCs on fiber substrates

Microscopic examination of cell morphology following initial cell seeding on the fiber substrates revealed that cell bodies elongate along the axis of the fiber and extend neurites that are guided by fiber directionality (Fig. 2a). Since the average diameter of individual fibers is substantially narrower than the dimensions of a cell, ANSCs cannot spread in an unrestricted manner on fiber substrates as they would on a planar surface. As a result, the intracellular cytoskeletal structure of ANSCs is likely altered as compared with planar surfaces, most notably resulting in cellular alignment along the dominant fiber axis. We were interested to investigate if this change in cell morphology would alter the cellular responsiveness to differentiation-inducing conditions.

To this end, ANSCs were seeded onto various PLO/LN-coated substrates and treated with RA/FBS to induce neuronal differentiation, and immunostained for the immature neuronal marker Tuj1 after five days. Tuj1+ cells on aligned fibers extended neurites several times the length of the cell body that were guided by the axis of fiber alignment (Fig. 2e). On the other hand, such cells on the random fiber meshes showed extensive, but randomly extended neurite fields (Fig. 2f).

The highest fractions of Tuj1+ cells were generated on aligned fiber substrates, with 47% of cells staining positive on the 480-nm aligned fibers (Fig. 3), 2.5-fold higher than on the similarly coated planar control ($p < 0.01$). In addition, all aligned substrates yielded greater fractions of Tuj1+ cells compared with random fibers of similar dimensions, suggesting that substrate alignment, rather than fibrous topography alone, was a major factor favoring the yield

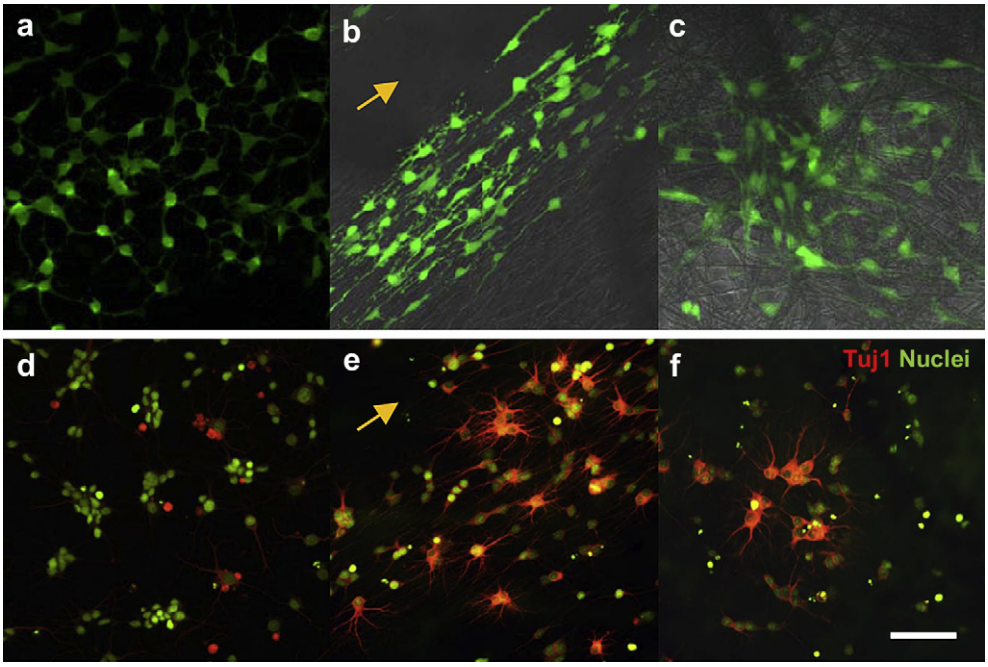


**Fig. 2.** Representative fluorescent images of ANSCs on planar surfaces and fiber substrates. Images were acquired at 200× magnification and the scale bar = 50 μm (a–c) GFP + ANSCs under continued proliferation conditions on planar TCPS (a), aligned 480-nm PCL fibers (b), and random 480-nm PCL fibers (c). (d–f) ANSCs after 5 days of differentiation following a single dose of 0.5 μM RA and 0.5% FBS treatment. Cell nuclei were labeled with SYTOX Green and early neurons were immunostained with anti-Tuj1 antibody (red). (d) Cells on planar TCPS; (e) aligned 480-nm PCL fibers; (f) random 480-nm PCL fibers. Arrows on images indicate direction of fiber alignment on relevant substrates.

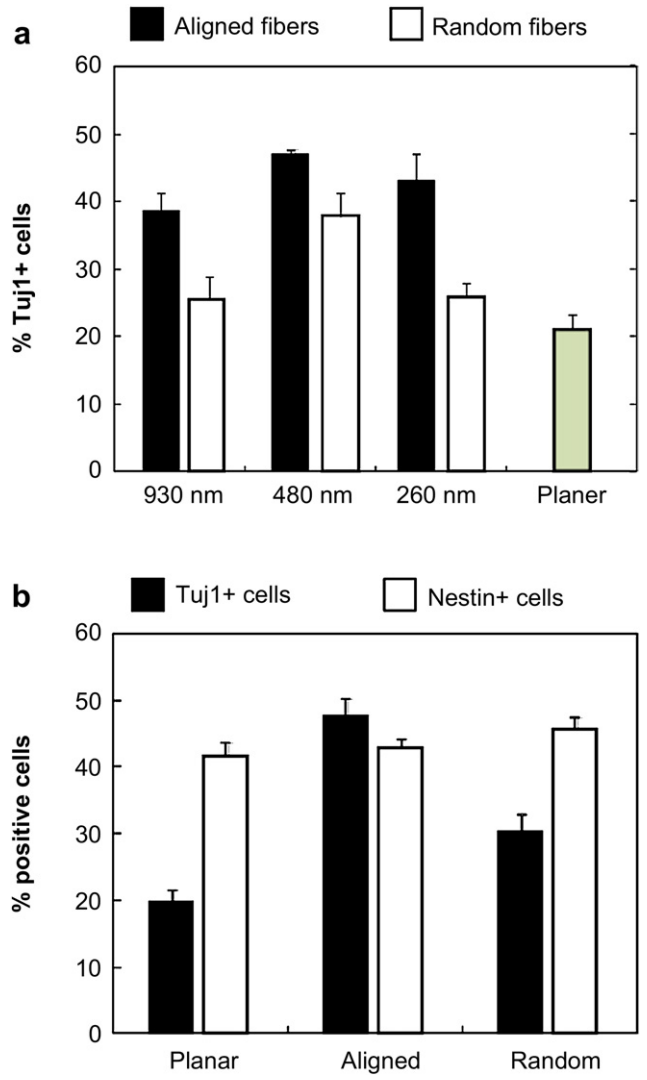


**Fig. 3.** Quantification of early neuronal differentiation on various substrates. Columns represent the mean ± standard error ($n = 5$) for each type of substrate. (a) % of Tuj1+ cells 5 days after RA/FBS differentiation at 12,500 cells/cm$^2$. (b) % of Tuj1+ and nestin+ cells on planar and 480-nm substrates 5 days after RA/FBS differentiation at 30,000 cells/cm$^2$.

of neuronal progenitors. Although percentages of Tuj1+ cells on 930-nm and 260-nm random fiber meshes were comparable to those on the planar substrate, ANSCs on the 480-nm random fibers had significantly greater neuronal differentiation 38% *vs.* 21% on TCPS, $p < 0.01$, pointing to the impact of feature size in influencing neuronal differentiation.

Expression of nestin, the marker for undifferentiated ANSCs, was also quantified to investigate the overall impact of fiber topography on loss of stemness and increased differentiation (data not shown). On planar surfaces, 45% of ANSCs remained nestin+, whereas only 30–35% of ANSCs on fiber substrates were nestin+. However, there was no statistically significant difference amongst all the fiber mesh groups. At the same time, expression of Ki-67, a proliferative marker, was slightly higher on all fiber substrates.

Taking into consideration that paracrine signaling from closely associated ANSCs might exert additional influence on differentiation and fate specification [23,24], a subsequent experiment was performed where cells were seeded at a threefold higher density prior to RA induction. The 480-nm substrate was selected for this test because both the aligned and random fibers at this dimension yielded the highest fractions of Tuj1+ cells, indicating that a topographical cue at this size scale provided the strongest pro-neuronal signal. In this instance, all substrates had a slight reduction in the fraction of Tuj1+ cells. 45% of ANSCs on aligned fibers were Tuj1+, which was still more than double the fraction on planar surface (18%) and also 17% greater than the random fibers ($p < 0.01$). All the substrates had ~40% nestin+ cells, which was slightly higher than observed under low-density differentiation conditions.

### 3.3. Oligodendrocyte survival and attachment on fiber substrates

Immunostaining for the other neural lineages showed that the fraction of ANSCs differentiating into astrocytes was <10%, regardless of the substrate topography. However, we previously observed that a significant proportion of ANSCs differentiated into RIP+ cells following withdrawal of FGF-2 from the culture media [25], suggesting that ANSCs in culture tend to favor an oligodendrocyte fate choice in the absence of extrinsically applied biochemical induction. We thus specifically tested the hypothesis that the enrichment of Tuj1+ cells on the fiber substrates was due to negative selection against oligodendrocytes.

Nearly 75% of ANSCs on culture dishes were found to differentiate into oligodendrocytes when differentiation was induced with a combination of 100 ng/ml noggin and 100 ng/ml IGF-1. This mixed population of cells was subsequently plated onto different fiber substrates and then allowed to attach for 24 h before further analysis. When the total cell population was quantified using the WST-1 metabolic assay, we observed cell viability on all the fiber substrates was less than on planar tissue culture surfaces, indicating that cell attachment efficacy and survival are influenced by substrate topography. There was a marked decrease in the number of cells adhered on aligned fibers as compared to random fiber substrates; notably, only half as many cells had adhered to the aligned fibers than on the planar substrate (Fig. 4a). Cell attachment and viability onto random fiber substrates was inversely correlated with increasing fiber diameter, where the largest fibers supported the poorest overall cell attachment. When the cell number on each substrate was multiplied by the average fraction of RIP+ cells, the data indicates that only about 40% of RIP+ cells had attached to the aligned fiber substrates.

In addition to having a negative impact on the initial attachment of oligodendrocytes, a potential means by which aligned fiber substrates may enrich Tuj1+ cell populations is through activation of apoptotic pathways in non-neuronal cells. Immunostained samples were thus counter-stained using the TUNEL assay, and the cells that showed double staining (RIP+ and TUNEL+) were scored. A baseline level of 5% of RIP+ cells on the 2D substrate were apoptotic. As the fiber diameter increased, the fraction of cells undergoing apoptosis increased. More significantly, aligned fiber substrates performed the poorest in terms of supporting RIP+ cell survival, with 9.5% of oligodendrocytes attached to 930-nm aligned fibers exhibiting apoptotic markers at 24 h post-seeding.

To verify that the phenomenon of substrate selectivity was specific for oligodendrocyte progenitors and not for neuronal progenitors, a subsequent experiment was performed whereby ANSCs on tissue culture plates were induced to differentiate into neuronal lineages via RA/FBS treatment for 5 days. These cells were then trypsinized and re-plated in the same manner as the oligodendroglial-differentiated cells. The analysis of total and Tuj1+ cell numbers and the TUNEL assay was repeated (Fig. 4e, f). In contrast to the IGF/noggin-treated cells, RA-treated cells showed relatively better attachment to fiber substrates compared with planar substrates following re-plating. The cells on fiber substrates also exhibited continued overall proliferation. Specifically, the number of Tuj1+ cells was elevated, indicating that fiber substrates were also supportive of proliferation of neuronal progenitors.

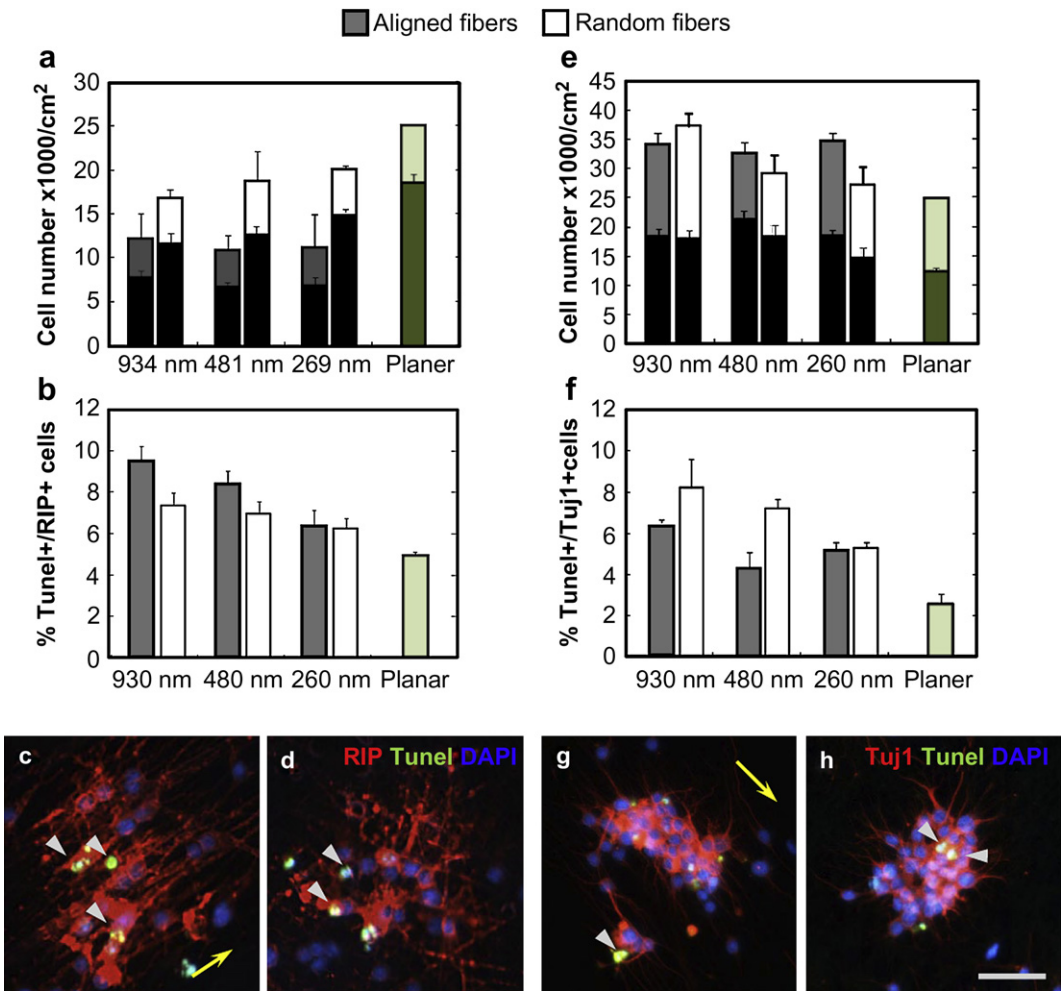


**Fig. 4.** Quantification of substrate selectivity to pre-differentiated cells. (a–d) ANSCs were differentiated using 100 ng/ml IGF and 100 ng/ml noggin for 5 days, and then seeded onto the substrates at 25,000/cm$^2$. Cells were analyzed and fixed for immunostaining after 24 h. (a) Total cell number on various substrates (dark bars: total number of RIP+ cells); (b) percentage of RIP+ cells that were also apoptotic; (c) representative image cells on aligned fiber substrate; (d) cells on random fiber substrate. (e–h) ANSCs were differentiated using RA/FBS for 5 days, and then seeded at 25,000/cm$^2$. Cells were analyzed and fixed for immunostaining after 24 h. (e) Total cell number on various substrates (dark bars: total number of Tuj1+ cells); (f) percentage of Tuj1+ cells that were also apoptotic; (g) cells on aligned fiber substrate; (h) cells on random fiber substrate. Arrows indicate direction of alignment and arrowheads indicate doubly stained (RIP+/apoptotic or Tuj1+/apoptotic) cells.

### *3.4. Activation of canonical Wnt/β-catenin signaling*

Activation of the canonical Wnt signaling pathway results in degradation or inhibition of axin and glycogen synthase kinase 3β (GSK3β); consequently, instead of undergoing rapid degradation, cytosolic β-catenin is allowed to accumulate and translocate to the nucleus. Nuclear β-catenin binds to the TCF/LEF promoter region to activate gene expression. A luciferase reporter construct was used to quantify the extent of Wnt/β-catenin activation in ANSCs in response to substrate topography. ANSCs were transiently transfected with reporter plasmids prior to re-plating onto fibrous scaffolds. We first verified the activity of the plasmid via Wnt3a treatment of transduced cells. ANSCs transduced with pGL3-OT reporter exhibited a minimum of 5-fold-increase in luciferase activity when stimulated with 150 ng/ml Wnt3a, whereas ANSCs transduced with the negative control reporter pGL3-OF did not express any luciferase signal above the background (not shown).

ANSCs on planar substrates showed a basal level of activation in the absence of additional biochemical cues (Fig. 5a). All luciferase activity readings were thus normalized and represented as a fold-increase over the basal activation. In the absence of any additional biochemical cues, ANSCs responded to fiber topography with an increase in canonical Wnt signaling. With the exception of the 930-nm random fibers, activation levels in all samples were at least twice of that of cells on planar substrate. Treatment of cells with RA/FBS further potentiated activation levels approximately one-fold over untreated samples in all the testing groups (Fig. 5b). There was a markedly higher level of signal activation in ANSCs cultured on aligned fibers than those on random fibers in the 480-nm and 930-nm groups. On the other hand, activation levels in the groups of 260-nm aligned and random fibers were comparable. Overall, signal activation was the lowest in ANSCs cultured on 930-nm random fibers, and highest in ANSCs on 480-nm aligned fibers. When cells were treated with soluble Wnt3a, ANSCs on 260-nm and 930-nm aligned fiber substrates showed similar activation levels to cells on the same substrates after RA/FBS treatment (Fig. 5c). ANSCs on both types of 480-nm substrates were activated to a higher degree by soluble Wnt3a than by RA/FBS treatment.

## 4. Discussion

The phenomenon of contact guidance of neural cells via substratum topography has numerous correlates *in vivo*, such as guidance of axons along the bands of Büngner and endoneurial tubes during peripheral nerve regeneration [26,27], as well as

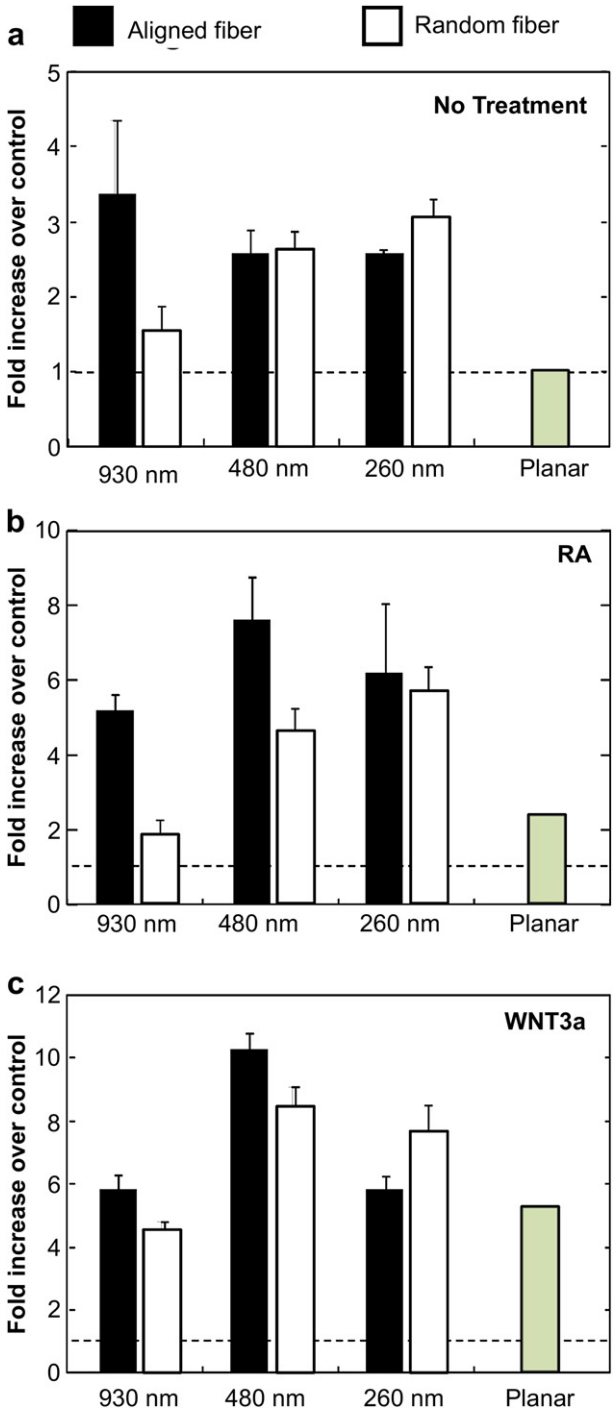


**Fig. 5.** Activation of canonical Wnt/β-catenin signaling as measured using the TOPFLASH luciferase reporter assay. Luciferase readings were normalized to protein concentration of the sample. Readings are presented as fold-increase over the luciferase activity of untreated ANSCs seeded onto planar TCPS substrates (dotted line on each graph). (a) ANSCs without any treatment; (b) ANSCs treated with 0.5 μM RA and 0.5% FBS; (c) ANSCs treated with 150 ng/ml Wnt3a.

migration of oligodendrocyte and neuronal precursor cells towards forebrain targets in the developing central nervous system [28–30]. It has been previously established that such guidance may be mediated via specific cell–cell or cell–ECM contacts including cadherins, integrins and neural cell adhesion molecules. On the other hand, it also raises a question whether nanofibrous extracellular features are capable of altering cell behavior by inducing morphological changes with downstream intracellular signaling consequences. However, despite the vast body of pre-existing work demonstrating that topographical control of stem cells with synthetic substrates *in vitro* is achievable [31,32], there has been little follow-up to date delving into possible mechanistic explanations for the observed phenomena.

Here, we have shown that the response of ANSCs to exogenous differentiation cues can be modulated by the topography of the substratum, when presented as either aligned or random electrospun fibrous substrates with diameters in the hundreds of nanometers, or approximately 1/40–1/10 of the diameter of a rounded ANSC. In the presence of RA/FBS as an inducer of neuronal differentiation, culturing ANSCs on aligned fibers significantly potentiated the yield of cells with a neuronal fate specification, as compared to random fibrous or planar substrates. Fibrous topographies in general were more permissive to differentiation, as indicated by the concomitant decrease in the fraction of cells remaining in the progenitor stage. Furthermore, substrate topography was transmitted to the ANSCs, which elongated and extended highly directional neurites along the axis of fiber alignment, but stayed rounder with extensive neurite fields on random fibers. There also appeared to be a fiber size dependency in the efficiency of neuronal differentiation, with 480 nm fibers yielding the highest fraction of Tuj1+ cells on both aligned and random fibers, respectively. This suggests a unique sensitivity of ANSCs to substrate feature size that is worthy of future investigation. The pro-neuronal cue offered by the 480 nm aligned fiber persists even under conditions of high-density differentiation, which was previously thought to provide a greater degree of paracrine signaling that would promote maintenance of stemness in ANSCs. Indeed, Tuj1+ cells found on planar and random fiber substrates decreased as compared with the low-density conditions, but maintained on the aligned fibers, indicating that fiber topography posed a stronger signaling cue than soluble paracrine signaling from neighboring cells. Based on these findings, we postulated two mechanisms that could be responsible for the observed enrichment of neuronal cells: firstly, the aligned substrate topography was favorable to the attachment and survival of neuronal progenitors and conversely unfavorable to non-neuronal cell types; secondly, the fiber topography altered the pattern of cell-substrate contacts, resulting in cytoskeletal rearrangements and subsequently leading to changes in intracellular signaling activation.

To investigate the substrate selectivity hypothesis, we evaluated the attachment and survival of two different cell populations, one that was selectively differentiated to yield a large fraction of oligodendrocytes (2 doses of IGF/noggin for 5 days), and another that was selectively differentiated into early neurons (2 doses of RA/FBS over 5 days). Fiber substrates in general were less receptive to the attachment of predominantly oligodendrocyte cell population, most notably on aligned substrates. In addition, the continued survivability of oligodendrocytes on these substrates was low, with increased fraction of RIP+ cells staining positively for apoptosis. On the other hand, attachment and viability of RA/FBS-treated populations of cells on fiber substrates were comparable to, or slightly better than on planar culture surfaces. Although there was a slightly elevated fraction of apoptotic Tuj1+ cells found on the fiber substrates, the overall numbers were lower than oligodendrocyte populations. Our data collectively suggests that one mechanism by which neuronal cells are enriched by the aligned topography is via selection against cells that have differentiated to other lineages, while substrate alignment favors neuronal cell morphology and thus cell survival. Rearrangement of focal adhesions and lack of cell spreading in response to substrate-presented cues have been linked to activation of apoptotic pathways, either via canonical FAK signaling or non-canonical pathways such as p53 [33–35]. The concept of selective apoptosis within the developing

nervous system is well-established, whether as a means of matching innervation with target cell population or removal of transiently functional or erroneous connections [36]. In this context, apoptosis-activating signals are typically the addition or withdrawal of trophic molecules; however, we speculate that topographical cues might be an alternative means of selecting for a specific neural stem cell fate choice.

In addition to dictating cell fate between survival and apoptosis, substrate topography has also been shown to effect changes in gene expression (e.g. expression of markers of cell differentiation) via cytoskeletal or nuclear elongation [37–39]. Distortion of the nucleus was shown to correlate with decreased proliferation and increased osteocalcin gene expression in primary osteogenic cells, and cell elongation on 350-nm gratings resulted in neural transdifferentiation of MSCs with corresponding upregulation of MAP2 expression [40]. Signaling through the canonical β-catenin/Wnt signaling pathway is crucial for a number of developmental roles, including neurogenesis in both embryonic and adult neural precursor cells [41–44]. Due to the dual-functional nature of β-catenin as a structural component of the cytoskeleton as well as mediator of canonical Wnt signaling, it is possible that structural rearrangements in ANSC morphology in response to nanotopographical cues could influence the dynamics of intracellular β-catenin bioavailability. Yarema and colleagues have previously shown that differential cell adhesion resulting from surface expression of thiolated synthetic sugar analogs increased the nuclear localization of β-catenin in human embryoid body-derived cells [45]. MSCs that were confined to patterns that increased cell contractility, such as star or elongated shapes, also showed upregulation in both canonical and non-canonical Wnt gene expression [46]. Here, we probed TCF/LEF activation in ANSCs and found that in the absence of soluble cues, fiber topography itself was sufficient to drive the activation of canonical Wnt signaling. Treatment of ANSCs with RA potentiated activation by another one-fold, although these levels remained lower across the board compared to direct stimulation by treatment with soluble recombinant Wnt3a. Upregulation of NeuroD signaling in response to RA was shown to promote neuronal differentiation in ANSCs [20]; furthermore, recent work established that Wnt/β-catenin signaling with simultaneous Sox2 silencing also triggered NeuroD activation [47]. Potentiation of the neurogenic program via topographically induced Wnt signaling might thus be responsible for the enhancement of neuronal differentiation from ANSCs on aligned fiber substrates.

## 5. Conclusions

Stem cells have been shown to alter their morphology in response to underlying substrate topography, with subsequent consequences on cell fate such as proliferation, survival, and differentiated gene expression. In this study, we probed the effects of fibrous substrate topography on neuronal differentiation of ANSCs. Substrate-induced cell elongation and alignment increased the efficiency of neuronal differentiation, with 480-nm aligned fiber meshes yielding the highest fraction of neuronal progenitors. This effect was found to be due to the combined effect of substrate selectivity against oligodendrocytes as well as substrate-mediated increase in canonical Wnt signaling. Although this study has provided some mechanistic insight into how substrate topography can influence stem cell differentiation, future studies will be focused on clarifying the intermediate steps connecting intracellular structural changes and downstream signaling pathways in response to external topographical cues.

## Acknowledgments

Financial support for this study was provided by the National Science Foundation Early Career Award (DMR-0848340, H.Q.M.), Maryland Stem Cell Research Commission (2007-MSCRFE-018 and 2009-MSCRFE-0084, H.Q.M.) and the National Institute of Biomedical Imaging and Bioengineering (EB005692, K.J.Y.). H.S. was partially supported by NS047344. S.H.L. acknowledges the support of the Siebel Foundation. X.Y.L. is a recipient of the Maryland Stem Cell Postdoctoral Fellowship.

## Appendix

Figures with essential color discrimination. Figs. 2–5 in this article have parts that are difficult to interpret in black and white. The full colour images can be found in the online version, at doi:10.1016/j.biomaterials.2010.08.021.

## References

[1] Domian IJ, Chiravuri M, van der Meer P, Feinberg AW, Shi X, Shao Y, et al. Generation of functional ventricular heart muscle from mouse ventricular progenitor cells. Science 2009;326:426–9.
[2] Shah RN, Shah NA, Del Rosario Lim MM, Hsieh C, Nuber G, Stupp SI. Supramolecular design of self-assembling nanofibers for cartilage regeneration. Proc Natl Acad Sci U S A 2010;107:3293–8.
[3] Cui L, Jiang J, Wei L, Zhou X, Fraser JL, Snider BJ, et al. Transplantation of embryonic stem cells improves nerve repair and functional recovery after severe sciatic nerve axotomy in rats. Stem Cells 2008;26:1356–65.
[4] Kemp SW, Walsh SK, Midha R. Growth factor and stem cell enhanced conduits in peripheral nerve regeneration and repair. Neurol Res 2008;30:1030–8.
[5] Gao L, McBeath R, Chen CS. Stem cell shape regulates a chondrogenic versus myogenic fate through Rac1 and N-cadherin. Stem Cells 2010;28:564–672.
[6] Engler AJ, Sen S, Sweeney HL, Discher DE. Matrix elasticity directs stem cell lineage specification. Cell 2006;126:677–89.
[7] McBeath R, Pirone DM, Nelson CM, Bhadriraju K, Chen CS. Cell shape, cytoskeletal tension, and RhoA regulate stem cell lineage commitment. Dev Cell 2004;6:483–95.
[8] Reilly GC, Engler AJ. Intrinsic extracellular matrix properties regulate stem cell differentiation. J Biomech 2010;43:55–62.
[9] Gerecht S, Bettinger CJ, Zhang Z, Borenstein JT, Vunjak-Novakovic G, Langer R. The effect of actin disrupting agents on contact guidance of human embryonic stem cells. Biomaterials 2007;28:4068–77.
[10] Chen CS. Mechanotransduction – a field pulling together? J Cell Sci 2008;121:3285–92.
[11] Flemming RG, Murphy CJ, Abrams GA, Goodman SL, Nealey PF. Effects of synthetic micro- and nano-structured surfaces on cell behavior. Biomaterials 1999;20:573–88.
[12] Curtis A, Wilkinson C. Topographical control of cells. Biomaterials 1997;18:1573–83.
[13] Yim EK, Leong KW. Significance of synthetic nanostructures in dictating cellular response. Nanomedicine 2005;1:10–21.
[14] Lie DC, Colamarino SA, Song HJ, Desire L, Mira H, Consiglio A, et al. Wnt signalling regulates adult hippocampal neurogenesis. Nature 2005;437:1370–5.
[15] Lin K, Chua KN, Christopherson GT, Lim S, Mao HQ. Reducing electrospun nanofiber diameter and variability using cationic amphiphiles. Polymer 2007;48:6384–94.
[16] Lim SH, Mao HQ. Electrospun scaffolds for stem cell engineering. Adv Drug Deliv Rev 2009;61:1084–96.
[17] Palmer TD, Takahashi J, Gage FH. The adult rat hippocampus contains primordial neural stem cells. Mol Cell Neurosci 1997;8:389–404.
[18] Song HJ, Stevens CF, Gage FH. Neural stem cells from adult hippocampus develop essential properties of functional CNS neurons. Nat Neurosci 2002;5:438–45.
[19] Gage FH, Coates PW, Palmer TD, Kuhn HG, Fisher LJ, Suhonen JO, et al. Survival and differentiation of adult neuronal progenitor cells transplanted to the adult brain. Proc Natl Acad Sci U S A 1995;92:11879–83.
[20] Takahashi J, Palmer TD, Gage FH. Retinoic acid and neurotrophins collaborate to regulate neurogenesis in adult-derived neural stem cell cultures. J Neurobiol 1999;38:65–81.
[21] Hsieh J, Aimone JB, Kaspar BK, Kuwabara T, Nakashima K, Gage FH. IGF-1 instructs multipotent adult neural progenitor cells to become oligodendrocytes. J Cell Biol 2004;164:111–22.
[22] Shih IM, Yu J, He TC, Vogelstein B, Kinzler KW. The beta-catenin binding domain of adenomatous polyposis coli is sufficient for tumor suppression. Cancer Res 2000;60:1671–6.
[23] Tropepe V, Sibilia M, Ciruna BG, Rossant J, Wagner EF, van der Kooy D. Distinct neural stem cells proliferate in response to EGF and FGF in the developing mouse telencephalon. Dev Biol 1999;208:166–88.
[24] Taupin P, Ray J, Fischer WH, Suhr ST, Hakansson K, Grubb A, et al. FGF-2-responsive neural stem cell proliferation requires CCG, a novel autocrine/paracrine cofactor. Neuron 2000;28:385–97.
[25] Song H, Stevens CF, Gage FH. Astroglia induce neurogenesis from adult neural stem cells. Nature 2002;417:39–44.
[26] Thomas PK. Changes in the endoneurial sheaths of peripheral myelinated nerve fibres during Wallerian degeneration. J Anat 1964;98:175–82.

[27] Thomas PK, Sheldon H. Tubular arrays derived from myelin breakdown during Wallerian degeneration of peripheral nerve. J Cell Biol 1964;22:715–8.
[28] Temple S. The development of neural stem cells. Nature 2001;414:112–7.
[29] Levison SW, Chuang C, Abramson BJ, Goldman JE. The migrational patterns and developmental fates of glial precursors in the rat subventricular zone are temporally regulated. Development 1993;119:611–22.
[30] Hatten ME. Central nervous system neuronal migration. Annu Rev Neurosci 1999;22:511–39.
[31] Bettinger CJ, Langer R, Borenstein JT. Engineering substrate topography at the micro- and nanoscale to control cell function. Angew Chem Int Ed Engl 2009;48:5406–15.
[32] Guilak F, Cohen DM, Estes BT, Gimble JM, Liedtke W, Chen CS. Control of stem cell fate by physical interactions with the extracellular matrix. Cell Stem Cell 2009;5:17–26.
[33] Ilic D, Almeida EA, Schlaepfer DD, Dazin P, Aizawa S, Damsky CH. Extracellular matrix survival signals transduced by focal adhesion kinase suppress p53-mediated apoptosis. J Cell Biol 1998;143:547–60.
[34] Re F, Zanetti A, Sironi M, Polentarutti N, Lanfrancone L, Dejana E, et al. Inhibition of anchorage-dependent cell spreading triggers apoptosis in cultured human endothelial cells. J Cell Biol 1994;127:537–46.
[35] Chen CS, Mrksich M, Huang S, Whitesides GM, Ingber DE. Geometric control of cell life and death. Science 1997;276:1425–8.
[36] Yuan J, Yankner BA. Apoptosis in the nervous system. Nature 2000;407:802–9.
[37] Thomas CH, Collier JH, Sfeir CS, Healy KE. Engineering gene expression and protein synthesis by modulation of nuclear shape. Proc Natl Acad Sci U S A 2002;99:1972–7.
[38] Chew SY, Mi R, Hoke A, Leong KW. The effect of the alignment of electrospun fibrous scaffolds on Schwann cell maturation. Biomaterials 2008;29:653–61.
[39] Oh S, Brammer KS, Li YS, Teng D, Engler AJ, Chien S, et al. Stem cell fate dictated solely by altered nanotube dimension. Proc Natl Acad Sci U S A 2009;106:2130–5.
[40] Yim EK, Pang SW, Leong KW. Synthetic nanostructures inducing differentiation of human mesenchymal stem cells into neuronal lineage. Exp Cell Res 2007;313:1820–9.
[41] Kasai M, Satoh K, Akiyama T. Wnt signaling regulates the sequential onset of neurogenesis and gliogenesis via induction of bmps. Genes Cells 2005;10:777–83.
[42] Inestrosa NC, Arenas E. Emerging roles of Wnts in the adult nervous system. Nat Rev Neurosci 2010;11:77–86.
[43] Agathocleous M, Iordanova I, Willardsen MI, Xue XY, Vetter ML, Harris WA, et al. A directional Wnt/beta-catenin-Sox2-proneural pathway regulates the transition from proliferation to differentiation in the xenopus retina. Development 2009;136:3289–99.
[44] Gulacsi AA, Anderson SA. Beta-catenin-mediated Wnt signaling regulates neurogenesis in the ventral telencephalon. Nat Neurosci 2008;11:1383–91.
[45] Sampathkumar SG, Li AV, Jones MB, Sun Z, Yarema KJ. Metabolic installation of thiols into sialic acid modulates adhesion and stem cell biology. Nat Chem Biol 2006;2:149–52.
[46] Kilian KA, Bugarija B, Lahn BT, Mrksich M. Geometric cues for directing the differentiation of mesenchymal stem cells. Proc Natl Acad Sci U S A 2010;107:4872–7.
[47] Kuwabara T, Hsieh J, Muotri A, Yeo G, Warashina M, Lie DC, et al. Wnt-mediated activation of NeuroD1 and retro-elements during adult neurogenesis. Nat Neurosci 2009;12:1097–105.